Optical and thermodynamic properties of the high-temperature superconductor $HgBa_2CuO_{4+\delta}$

E. van Heumen,[1] R. Lortz,[1] A.B. Kuzmenko,[1] F. Carbone,[1] D. van der Marel,[1] X. Zhao,[2] G. Yu,[2] Y. Cho,[2] N. Barisic,[2] M. Greven,[2] C.C. Homes,[3] and S.V. Dordevic[3,4]

[1] *University of Geneva, 24, Quai E.-Ansermet, Geneva 4, Switzerland*
[2] *Department of Physics, Applied Physics, and Stanford Synchrotron Radiation Laboratory, Stanford University, Stanford, CA 94305*
[3] *Condensed Matter Physics & Materials Science Department, Brookhaven National Laboratory, Upton, New York 11973, USA*
[4] *Current adress: Department of Physics, The University of Akron, Akron, OH 44325, USA.*

(Dated: February 3, 2008)

In- and out-of-plane optical spectra and specific heat measurements for the single layer cuprate superconductor $HgBa_2CuO_{4+\delta}$ (Hg-1201) at optimal doping (T_c = 97 K) are presented. Both the in-plane and out-of-plane superfluid density agree well with a recently proposed scaling relation $\rho_s \propto \sigma_{dc} T_c$. It is shown that there is a superconductivity induced increase of the in-plane low frequency spectral weight which follows the trend found in underdoped and optimally doped $Bi_2Sr_2CaCu_2O_{8+\delta}$ (Bi-2212) and optimally doped $Bi_2Sr_2Ca_2Cu_3O_{10+\delta}$ (Bi-2223). We observe an increase of optical spectral weight which corresponds to a change in kinetic energy $\Delta W \approx$0.5 meV/Cu which is more than enough to explain the condensation energy. The specific heat anomaly is 10 times smaller than in $YBa_2Cu_3O_{6+\delta}$ (YBCO) and 3 times smaller than in Bi-2212. The shape of the anomaly is similar to the one observed in YBCO showing that the superconducting transition is governed by thermal fluctuations.

PACS numbers: 74.25.Bt, 74.25.Gz, 74.72.-h, 74.72.Jt, 78.30.-j

I. INTRODUCTION

In the 20 years after the discovery of high-temperature superconductivity the determination of the generic properties of these compounds has often been complicated by material and crystallographic issues. Examples are the structural distortion in Bi-2201, bi-layer splitting of the electronic bands due to multiple copper-oxygen sheets per unit cell and the copper-oxygen chains present in YBCO. In order to obtain information on the phenomenon of superconductivity in the high T_c cuprates that is free from these complications one would like to study the simplest possible structure. The mercury based cuprates with their simple tetragonal structure and in particular Hg-1201, with only one copper-oxygen sheet per unit cell and the highest T_c (≈97 K) of the single layer compounds, seem to be good candidates to achieve this goal. Moreover the critical temperatures of these compounds are the highest obtained to date. There are however some indications for intrinsic disorder in these compounds.[1] These systems have not been as extensively studied as other families because until recently sizeable single crystals were lacking. In an earlier publication[1] the successful growth of large single crystals of optimally doped, single-layer Hg-1201 has been reported. These crystals have subsequently been studied with resonant inelastic x-ray scattering[2] and ARPES.[3] In this paper we present optical properties of one such a sample together with measurements of the specific heat. The paper is organized as follows: in section II some sample related issues are discussed; section III explains the experimental techniques used and in section IV the results are presented and discussed. The conclusions are summarized in section V.

II. SAMPLE

Large single crystals were grown using an encapsulation process as discussed elsewhere.[1] The sample used for the in-plane measurements is oriented with its largest surface along the a-b plane with dimensions of $1.1 \times 1.4 \times 0.5$ mm^3. Magnetic susceptibility measurements give a critical temperature $T_c \approx$ 97 K with a somewhat broadened transition width of 5 K. The misorientation of crystallites is about 0.04°.[1] Hg-1201 is highly hygroscopic and does not cleave naturally along the ab-plane. Therefore we polished the sample with a 0.1 μm diamond abrasive in a pure nitrogen atmosphere before inserting it into the cryostat.

III. EXPERIMENTS

A. Optical measurements

In-plane normal incidence reflectivity measurements have been performed on a Fourier transform spectrometer in the frequency range between 100 - 7000 cm^{-1} (12 - 870 meV) coating the sample *in-situ* with gold to obtain a reference. Ellipsometric measurements were made on a Woolam VASE ellipsometer in the frequency range between 6000 and 30000 cm^{-1} (0.75 - 3.72 eV) which yield directly the real and imaginary parts of the dielectric

function $\epsilon(\omega)$. The spectra are taken with 2 K intervals between 20 K and 300 K. Two home made cryostats are used that stabilize the sample position during thermal cycling. They operate at pressures in the order of 10^{-6} mbar in the infrared region and 10^{-9} mbar in the visible light region. Figure 1a shows the in-plane reflectivity $R_{ab}(\omega)$ for selected temperatures. The reflectivity curves above 6000 cm^{-1} have been calculated from the dielectric function. Also shown is the reflectivity calculated from the pseudo dielectric function (see below).

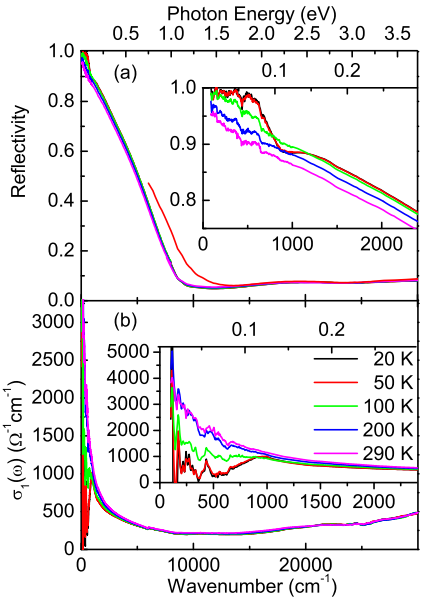

FIG. 1: (Color online)(a): In-plane reflectivity for selected temperatures. The reflectivity above 6000 cm^{-1} has been calculated from the measured dielectric function. The thin red curve is the reflectivity at room temperature calculated from the pseudo dielectric function. The inset shows the far infrared reflectivity. (b): In-plane optical conductivity $\sigma_1(\omega)$ for selected temperatures. The inset shows the low frequency part on an expanded scale. Some sharp structures in the region below 700 cm^{-1} are due to the remnants of the c-axis phonons. The temperatures are the same in all panels and are indicated in the inset in fig 1b.

In addition, the c-axis reflectivity $R_c(\omega)$ was measured on the ac-plane of a different sample from 30 to 20000 cm^{-1}. Figure 2a shows the c-axis reflectivity for selected temperatures. The c-axis optical conductivity is obtained from a Kramers-Kronig (KK) transformation and is shown in figure 2b. In table I the oscillator parameters for the 5 phonon lines are summarized. From a simple counting of atoms 8 phonon modes are expected of which only four should be infrared active. Comparing with other cuprates we attribute the first two phonon lines to Hg and Ba vibrations, the mode at 355 cm^{-1} to vibration of the in-plane oxygens and the highest mode at 622 cm^{-1} with the vibration of the apical oxygen mode. The fact that this mode is split indicates that

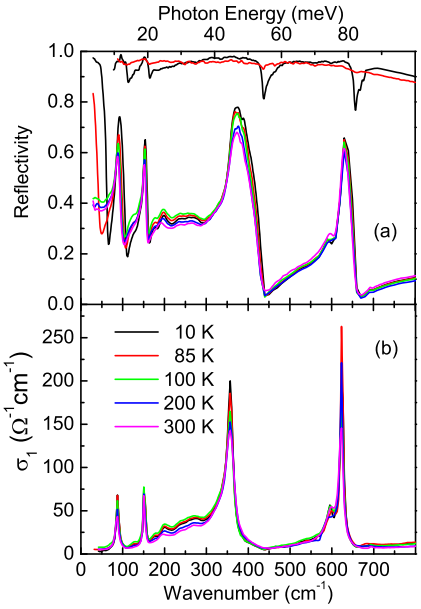

FIG. 2: (Color online) (a): Far infrared c-axis reflectivity at selected temperatures. Also shown is the in-plane reflectivity at 20 K measured with (red) and without polarizer (black). (b): The c-axis optical conductivity $\sigma_1(\omega)$. The temperatures are the same in all panels and are indicated in the inset in fig 2b.

there is some oxygen disorder present. The additional weak structure seen between 200 cm^{-1} and 300 cm^{-1} is probably also due to disorder. Below T_c a Josephson plasma edge appears that shifts with temperature to a maximum of around 70 cm^{-1} for the lowest measured temperature of 10 K.

The ellipsometric measurements were performed with an angle of incidence of 60°. Due to the large angle of incidence the measured pseudo dielectric function has an admixture of the c-axis component. The c-axis dielectric function derived from the c-axis reflectivity measurements was used to obtain the true in-plane dielectric function $\epsilon_{ab}(\omega)$, by an inversion of the Fresnel equations. The uncorrected dielectric function at room temperature and corrected dielectric function for several temperatures are shown in figure 3. Measurements were also performed for angles of incidence of 65°, 70° and 80° and no dependence of the corrected $\epsilon_{ab}(\omega)$ on the angle was found showing the consistency of this procedure.

A disadvantage of using a cut and polished surface as compared to a naturally cleaved one is the possible occurrence of a misorientation of the crystal axes relative to the sample surface. This results in the appearance of c-axis spectral features in the in-plane reflectivity spectra.[4] In figure 2a, R_{ab} measured with unpolarized light is shown. A comparison with R_c suggests that these features correspond to c-axis phonons. Also shown is a spectrum where a polarizer was oriented such that the spectral features observed in the first spectrum are minimized. Us-

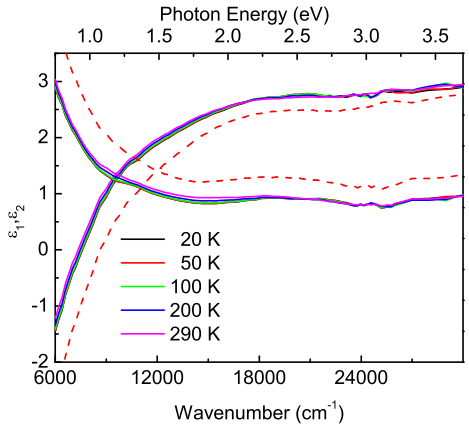

FIG. 3: (Color online) Dielectric function at selected temperatures corrected for the c-axis contribution using the method explained in the text. The pseudo dielectric function at room temperature are indicated by the thin red curves.

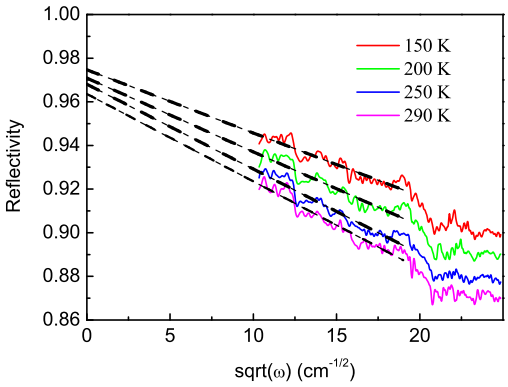

FIG. 4: (Color online) Reflectivity plotted versus $(\omega/2\pi c)^{1/2}$ and the fitted extrapolations (dashed) to zero frequency.

ing the model of Ref[4] the misorientation is estimated to be of the order of 3°. In order to suppress the c-axis phonon features in $R_{ab}(\omega)$, light polarized along the intersection of sample surface and ab-plane is used for the in-plane measurements. The features are not completely suppressed however, likely due to the finite angle of incidence (8°). This shows up in the optical conductivity and the extended Drude analysis below.

Another experimental issue is related to the absolute value of the in-plane reflectivity at low frequencies. In a metal for frequencies $\omega \ll 1/\tau$ one can use the Hagen-Rubens approximation[5] to describe the reflectance:

$$R(\omega) \simeq 1 - 2\left(\frac{2\omega}{\pi\sigma_0}\right)^{1/2}. \qquad (1)$$

Here σ_0 is the dc conductivity. This is also expected to approximately hold for cuprates in the normal state and this approximation is frequently used to perform KK transformations of reflectivity spectra. In figure 4 the in-plane reflectivity plotted versus $(\omega/2\pi c)^{1/2}$ is shown for four different temperatures in the normal state. The extrapolations have been obtained by fitting Eq. 1 to the spectra between 100 cm^{-1} and 300 cm^{-1}. One can see that the reflectivity extrapolates to ≈ 0.97 instead of 1 for $\omega \to 0$. Since the curves all extrapolate to approximately the same value the difference is presumably due to the presence of a non-conducting secondary phase. From the fits we extracted the dc conductivity and compared the temperature dependence to resistivity measurements.[6] These two measurements correspond in absolute value and follow the same temperature dependence. However a problem arises when we try to model R_{ab} with a Drude-lorentz model. For temperatures below T_c the fits show no sign of superconductivity. Instead of a delta function or very narrow Drude like contribution we find a rather broad Drude peak. Moreover the temperature dependence of the dc conductivity obtained from the model does not correspond with the resistivity measurements. We find that if we scale the in-plane reflectivity measurements upwards by 3% for all temperatures the dc conductivity extracted from the model closely follows the dc resistivity measurements and the Drude peak below T_c is replaced by a delta function.

To extract the optical conductivity from the measured in-plane reflectivity and dielectric function a KK constrained variational analysis is used.[7] First, $R_{ab}(\omega)$ and $\epsilon_{ab}(\omega)$ are fitted simultaneously to a standard Drude-Lorentz model of which the parameters are given in table I for the room temperature spectra. Note that the last oscillator falls outside the measured spectral range. In a second step this model is then refined using multi-

ϵ_∞	ω_o	ω_p	Γ	ω_o	ω_p	Γ
2.53	0	1.5	0.13	86	150	10
	0.48	1.34	0.9	151	140	5
	1.41	0.44	0.67	355	475	22
	2.51	1.54	1.78	595	300	35
	3.36	0.23	0.24	622	305	10
	4.87	3.92	2.21			

TABLE I: Left: Oscillator parameters of the in-plane room temperature Drude-Lorentz model in eV (except ϵ_∞ which is dimensionless). Right: c-axis phonon parameters in cm^{-1}

oscillator variational dielectric functions that fit all spectral details of $R_{ab}(\omega)$ and $\epsilon_{ab}(\omega)$. This approach improves the determination of the high frequency optical conductivity because the measured dielectric function in the visible light region is used to anchor the unknown phase of the reflectivity. The in-plane reflectivity measurements have been scaled upwards by 3% as explained above.

In figure 1b the optical conductivity is shown for selected temperatures. It displays many of the features common to cuprates. At room temperature the low fre-

quency spectrum is dominated by a Drude like peak that narrows when temperature is decreased. Below T_c a partial gap opens up followed by an onset in absorption that starts around 500 - 600 cm^{-1}. This value for the onset is comparable to optimally doped Bi-2212, YBCO and Tl-2201[8] which all have approximately the same critical temperature but very different crystal structures indicating that this onset originates in the CuO_2 planes. Above 0.5 eV the optical conductivity is only weakly temperature dependent. We find evidence for at least three interband transitions with resonance energies of 1.41 eV, 2.51 eV and 3.36 eV. The latter two transitions have resonance energies close to resonances observed in the RIXS study of Ref[2]. Unfortunately, the c-axis contamination of the in-plane spectra prevents us from making rigorous statements about any in-plane phonon features.

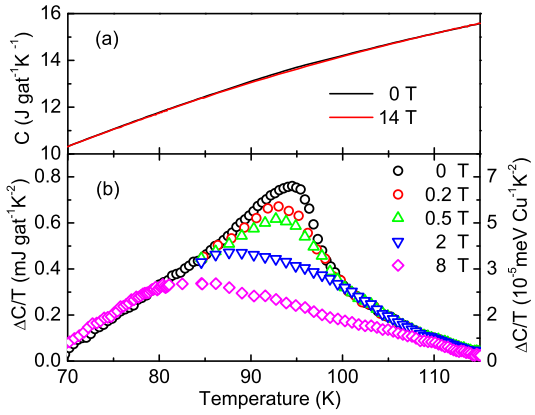

FIG. 5: (Color online) Difference of the specific heat data $\Delta C/T = (C(B,\mathrm{T}) - C(14T,\mathrm{T}))/T$ for a number of magnetic fields B showing the anomaly at the superconducting transition.

B. Specific heat measurements

Specific-heat measurements have been performed in magnetic fields up to 14 T on a small piece broken from the crystal used for the optical measurements with a mass of ∼700 μg. The magnetic fields used in these measurements are oriented perpendicular to the Cu-O planes. Since the specific heat is a probe of bulk thermodynamic properties the measurements confirm the bulk nature of the superconducting transition. It also gives an estimate of the strength of thermal fluctuations and of the superconducting condensation energy. A micro-relaxation calorimeter adapted to the small size of the crystal was used. Data has been taken using a generalized long relaxation method as described elsewhere.[9] This method gives a high precision in the determination of absolute values and a sensitivity comparable to that of standard AC methods as used in previous publications on Hg-1201.[10,11] The absolute error is estimated as 5 % due to the mass of the thermal compound used to mount the small sample. This does not enter into relative measurements when data taken in a magnetic field is used as a background.

In figure 5a we show two representative specific heat curves measured in fields of 0 T and 14 T. Figure 5b shows the difference $\Delta C/T$ between measurements taken in a field B and that taken in a field of 14 T in C/T. Due to the much higher upper critical field, subtracting data taken in a 14 T field does not provide the exact compensation of the phonon background but helps to investigate the shape and size of the anomaly. Note that the anomaly is only 0.4 % of the total specific heat and thus particularly small as compared to other cuprate superconductors.

IV. RESULTS

A. Extended Drude analysis

The original Drude theory of non-interacting electrons assumes a frequency independent scattering rate $1/\tau = const.$ This assumption does not hold in systems where the charge carriers interact with a bosonic spectrum or where strong correlations are important. This theory was extended by Allen and Mikkelsen to include a frequency dependent scattering rate $1/\tau(\omega)$ in which the optical conductivity takes the form,[12]

$$\sigma(\omega,T) = \frac{1}{4\pi}\frac{\omega_p^2}{1/\tau(\omega,T) - i\omega m^*(\omega,T)/m_b}, \qquad (2)$$

with ω_p the bare plasma frequency of the free charge carriers, m^* the effective mass and m_b the band mass. Note that since $\sigma(\omega,T)$ is causal, $1/\tau(\omega,T)$ and $m^*(\omega,T)/m_b$ obey KK relations. Although $1/\tau(\omega,T)$ and $m^*(\omega,T)/m_b$ are simply related to the real and imaginary parts of $1/\sigma(\omega)$, there is a subtlety that one has to consider to reliably extract these two quantities from the data. This is best illustrated by expressing $1/\tau(\omega,T)$ and $m^*(\omega,T)/m_b$ in terms of the dielectric function $\epsilon(\omega) = \epsilon_1(\omega) + i\epsilon_2(\omega)$:

$$\frac{1}{\tau(\omega)} = \frac{\omega_p^2}{\omega}\frac{\epsilon_2(\omega)}{[\epsilon_{\infty,IR} - \epsilon_1(\omega)]^2 + \epsilon_2^2(\omega)} \qquad (3)$$

and

$$\frac{m(\omega)}{m_b} = \frac{\omega_p^2}{\omega^2}\frac{\epsilon_{\infty,IR} - \epsilon_1(\omega)}{[\epsilon_{\infty,IR} - \epsilon_1(\omega)]^2 + \epsilon_2^2(\omega)}. \qquad (4)$$

Here $\epsilon_{\infty,IR}$ is the contribution to the dielectric function in the infrared arising from interband transitions which

should not be taken into account in the single component approach. The subtlety is in the choice of $\epsilon_{\infty,IR}$ and ω_p. The choice of $\epsilon_{\infty,IR}$ is not so important at low energies where $|\epsilon_1| \gg \epsilon_{\infty,IR}$ but becomes important at higher energies. For example, early studies of the cuprates indicated that the scattering rate was linear in frequency up to energies as high as 1 eV,[13] but if $\epsilon_{\infty,IR}$ is chosen as below the scattering rate starts to show signs of saturation already around 0.5 eV.[14] Here the following convention is adopted: $\epsilon_{\infty,IR} = \epsilon_\infty + \sum_j S_j$ where the $S_j = \omega_{p,j}/\omega_{0,j}$ are the oscillator strengths of the interband transitions obtained from a Drude-Lorentz fit (see Table I) and ω_p is chosen such that $m^*(\omega,T)/m_b$ approaches unity at high energy (∼1 eV). This leads to the choice $\epsilon_{\infty,IR} \approx 3.6$ and $\omega_p \approx$16500 cm^{-1} in the present case. The value of $\epsilon_{\infty,IR}$ is slightly smaller than the ones found in Ref[14] for Bi-2212, likely due to the smaller volume fraction of oxygens in the unit cell. The contribution to the dielectric function from the polarizability of oxygen is easily calculated using the Clausius-Mossotti relation,

$$\epsilon_{\infty,IR} \approx 1 + \frac{4\pi N\alpha/V}{1-\frac{4\pi}{3}N\alpha/V} = 1 + \frac{\alpha_0}{1-\gamma\alpha_0} \qquad (5)$$

where N is the number of oxygens per unit cell, V is the unit cell volume and α is the polarizability of the oxygen atoms. In the second equality we have defined $\alpha_0 \equiv 4\pi N\alpha/V$. The factor $\gamma = 1/3$ appearing in the denominator is a geometrical factor for a cubic crystal structure which we keep for simplicity. For O^{2-} the ionic polarizability $\alpha \approx 3.88{\cdot}10^{-24}$ cm^3. Using unit cell parameters for Hg-1201 of $a \times b \times c = 3.85 \times 3.85 \times 9.5$ $\dot{A}$ and 4 oxygen atoms per unit cell we find $\epsilon_{\infty,IR} \approx 3.56$, which is fortuitously close to our estimate of 3.6 in view of the lesser agreement for Bi-2212 and Bi-2223 as we now show. For optimally doped Bi-2212 and optimally doped Bi-2223 we use $a{\times}b{\times}c = 5.4 \times 5.4 \times 30.8$ $\dot{A}$ and $a{\times}b{\times}c = 5.4 \times 5.4 \times 37.1$ $\dot{A}$ respectively. These are the cell parameters corresponding to 4 formula units, i.e. $N = 32$ and $N = 40$ oxygens respectively. This yields $\epsilon_{\infty,IR} \approx 5.16$ and $\epsilon_{\infty,IR} \approx 5.52$. These values are substantially larger than the estimated experimental values $\epsilon_{\infty,IR} \approx 4.5$ for Bi-2212[14] and $\epsilon_{\infty,IR} \approx 4.1$ for Bi-2223. Figure 6 shows $1/\tau(\omega)$ and $m^*(\omega)/m_b$ for selected temperatures. The scattering rate is strongly suppressed below 600 cm^{-1} for temperatures below T_c indicative of the opening of a gap. ARPES measurements on Hg-1201 show a maximum gap value of 30 meV, but there is some uncertainty in this value because no quasiparticle peak is observed around the anti-nodal direction.[3] From the optical measurements it is difficult to extract the gap value: simple s-wave BCS superconductors in the dirty limit show an onset in absorption associated with the superconducting gap at 2Δ. This onset is shifted to $2\Delta + \Omega_{ph}$, with Ω_{ph} a phonon resonance energy, if the coupling to phonons is included. It has been suggested that the onset seen in cuprates is shifted due to the interaction of the electrons with the magnetic resonance mode[15] by Ω_{mr} to $2\Delta + \Omega_{mr}$. The onset here is defined as the point where

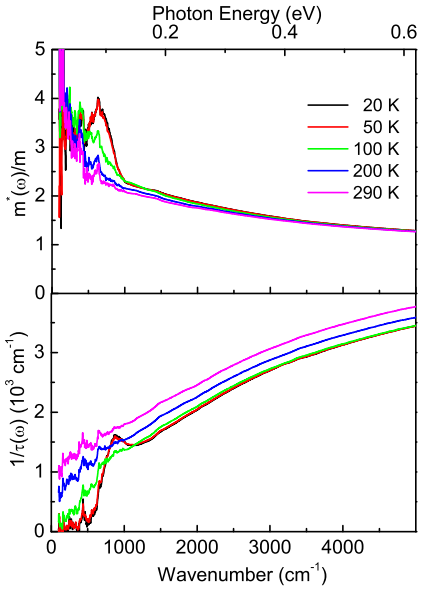

FIG. 6: (Color online) The frequency dependent scattering rate and effective mass of Hg-1201. The small peak in $m^*(\omega,T)/m_b$ at ≈ 620 cm^{-1} for temperatures above T_c is due to the remnant phonon structure.

the rise in $1/\tau(\omega)$ is steepest. This corresponds by KK relations to a maximum in $m^*(\omega)/m_b$. Using the values $\Omega_{mr} \approx 52 \pm 20$ meV[1] and $\Delta_0 \approx 30 \pm 10$ meV[3] we find $2\Delta + \Omega_{mr} \approx 110 \pm 30$ meV (900 ± 240 cm^{-1}), which is of the same order of magnitude as our experimental value of 80 ± 5 meV. In figure 7 the temperature dependence of $1/\tau(\omega,T)$ and $m^*(\omega,T)/m_b$ is shown for selected photon energies. In the normal state, the temperature dependence of $1/\tau(\omega,T)$ for small photon energies is linear in temperature but this linearity is lost for photon energies larger than $\hbar\omega > 0.1$ eV. The scattering rate shows a sharp drop at T_c for all photon energies except in a narrow window between 95 and 140 meV where the scattering rate increases below T_c. It has a maximum increase around 110 meV. The temperature dependence of $m^*(\omega,T)/m_b$ becomes roughly linear above $\hbar\omega > 0.1$ eV and shows an increase when the system becomes superconducting over most of the frequency range, except below 55 meV where it decreases.

B. Superfluid density

The in-plane condensate strength $\rho_s = \omega_{p,s}^2$ is determined in two ways. The first method is to fit the low temperature spectrum with a Drude-Lorentz model. In such a model the superfluid density is represented by a δ-peak at zero frequency with strength $\omega_{p,s}^2$. The value obtained from this method is $\omega_{p,s} = 9600 \pm 400$ cm^{-1} (1.2 ± 0.05 eV). The error bar on this quantity is determined by shifting the reflectivity up and down by 1 %

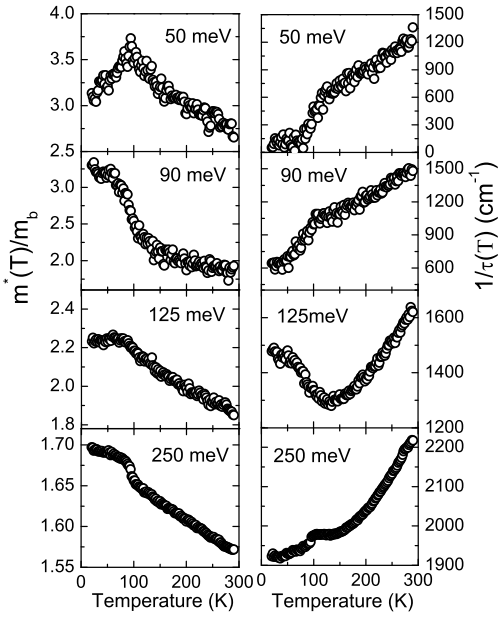

FIG. 7: Temperature dependence of $1/\tau(\omega,T)$ and $m^*(\omega,T)/m_b$ for selected energies. Both quantities show a clear departure from the normal state trend at T_c.

and observing the subsequent change in $\omega_{p,s}$. The corresponding values for Bi-2212 and Bi-2223 are $\omega_{p,s} = 9500$ cm^{-1} and $\omega_{p,s} = 10300$ cm^{-1} respectively.[31] The second method relies on the assumption that the real part of the dielectric function in the superconducting state is dominated at low frequencies by the superfluid density,

$$\epsilon_1(\omega) \approx -\frac{\omega_{p,s}^2}{\omega^2} \qquad (6)$$

Since $\epsilon_1(\omega)$ has been determined in a model independent way this result is more reliable. In figure 8 the function $-\omega^2\epsilon_1(\omega)$ is shown. The extrapolation to zero frequency of this function matches well with the value obtained with the Drude-Lorentz fit.

It is interesting to use the value for $\omega_{p,s}$ extracted from the in-plane measurements and from c-axis measurements to check the scaling relation $\rho_s \propto \sigma_{dc}T_c$.[16] This has already been done for the c-axis measurements in Ref. [16. From a Drude-Lorentz fit to the c-axis data a value of $\omega_{p,s} \approx 290 \pm 10$ cm^{-2} is found, more than a factor of 30 different from the in-plane value. At the same time from an extrapolation $\omega \to 0$ we find $\sigma_{1,c}(\omega \to 0, T \simeq T_c) \approx 7\ \Omega^{-1}$cm^{-1} for the c-axis and $\sigma_{1,ab}(\omega \to 0, T \simeq T_c) \approx 8300\ \Omega^{-1}$cm^{-1}. Put together we find $N_c \simeq 4.6\sigma_{dc}T_c$ and $N_{ab} \simeq 4.3\sigma_{dc}T_c$ in good agreement with the scaling trend observed in Ref[16].

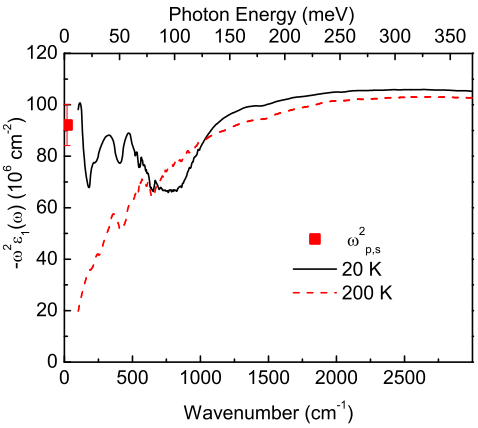

FIG. 8: $-\omega^2\epsilon_1(\omega)$ plotted at 20 K and 200 K . Extrapolating the 20 K curve to $\omega = 0$ agrees with the value $\omega_{p,s} = 9600 \pm 400$ cm^{-1} found from the Drude-Lorentz fit of the spectrum indicated by the square at ω= 0.

C. Low frequency spectral weight

In recent years there has been a lot of interest in the temperature dependence of the low frequency integrated spectral weight,

$$W(\Omega_c,T) = \int_0^{\Omega_c} \sigma_1(\omega,T)d\omega \approx \frac{\pi e^2 a^2}{2\hbar^2 V} < -\widehat{T} >, \qquad (7)$$

where a is the in-plane lattice constant, V the unit cell volume and $\widehat{T}$ the kinetic energy operator. Ω_c is a cut off frequency chosen to approximately separate the intraband and interband transitions. In a nearest neighbor tight binding model the relation between W(Ω_c,T) and $< -\widehat{T} >$ is exact. More recently it has been shown that this relation still holds approximately in the doping range under consideration.[17] According to BCS theory the kinetic energy increases when the system is driven into the superconducting state but it theoretically[18,19,20,21,22,23,24,25,26] and experimentally[27,28,29,30,31] it was found that in cuprates the kinetic energy decreases over a large doping range. Recently, in studies of the doping dependence of Bi-2212 it was found that on the overdoped side of the phase diagram the kinetic energy follows the BCS prediction.[32,33] Experimentally, $W(\Omega_c,T)$ gives a handle on the superconductivity induced change in kinetic energy. A qualitative indication of the superconductivity induced changes of low frequency spectral weight can be obtained from the dielectric function measured directly with ellipsometry. This can be done by monitoring the shift of the screened plasma frequency $\omega_p^* = \omega_p/\sqrt{\epsilon_\infty}$, *i.e* the frequency for which $\epsilon_1(\omega) = 0$, with temperature. Although it gives a first indication it does not give a definite answer since ω_p^* can be influenced by other factors, for instance the temperature dependence of the interband transitions. In figure 9, ω_p^* is plotted versus T^2.

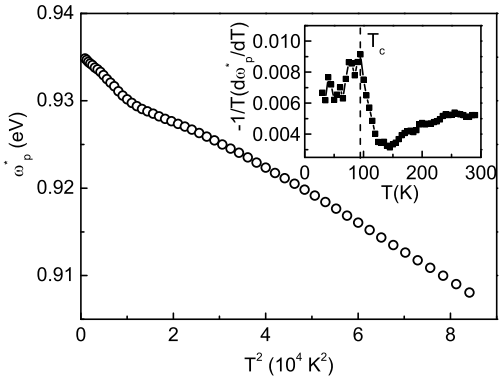

FIG. 9: Screened plasma frequency ω_p^* versus T^2. The relative error bars on this quantity are comparable to the size of the points. The inset shows the derivative.

The screened plasma frequency shows an extra blueshift below T_c, suggesting an increase of the low frequency spectral weight. Note that the absolute value of $\omega_p^*(\approx$ 7300 cm^{-1} at room temperature) is smaller than the one observed for optimally doped Bi-2212[28] ($\approx$ 7600 cm^{-1}) and Bi-2223[31] ($\approx$ 8100 cm^{-1}) which can be related to a smaller volume density of CuO_2 planes. In contrast to earlier observations ω_p^* shows a deviation from the T^2 behavior already in the normal state.

To calculate the integral in Eq. 7 one formally has to integrate from $\omega = 0$. Therefore to do the integration one has to rely on an extrapolation of the reflectivity to zero frequency. It has recently been shown that the superconductivity induced increase of spectral weight and absolute value of $W(\Omega_c, T)$ are rather insensitive to this extrapolation, provided one also uses the information contained in $\sigma_2(\omega, T)$.[31,34] Figure 10 shows the integrated spectral weight using Eq. 7 with the cut off Ω_c = 1 eV. One would like to choose Ω_c such that it separates the free carrier response from the bound charge response. This is strictly speaking not possible because in most cuprates the two regions overlap. Therefore the cut off is chosen in a region where the superconductivity induced change of spectral weight is more or less constant (figure 12c). By extrapolating the normal state trend to $T = 0$, the superconductivity induced increase of spectral weight is estimated to be $\Delta W \approx 1.5 \pm 1 \cdot 10^4$ Ω^{-1} cm^{-2} which is 0.5 % of the total spectral weight. A remark has to be made here on the temperature dependence of $W(\Omega_c, T)$. The temperature dependent reflectivity measurements show a hysteresis between curves measured cooling down and curves measured warming up for frequencies between 3000 cm^{-1} and 7000 cm^{-1}. This hysteresis is probably caused by a small amount of gas absorption on the sample surface. This has the effect of suppressing the reflectivity in this range below 150 K with a maximum suppression at 20 K of about 0.5 %. This trend was not observed in the ellipsometric data in the region of overlap. The upward kink at T_c is not affected by this, but the deviation from T^2 behavior below 150 K could be a result of this. Note that $W(\Omega_c, T)$ closely follows $\omega_p^*(T)$, so the temperature dependence of $W(\Omega_c, T)$ is probably not too much affected. In several other cuprates the temperature dependence of the normal state optical spectral weight is quadratic. Here we observe this quadratic temperature dependence only for temperatures higher than 170 K. The coefficient of this quadratic part has been observed to be unexpectedly large and is believed to be due to correlation effects.[23] To compare the superconductivity induced increase of $W(\Omega_c, T)$ to other compounds we express ΔW in meV/Cu. We find $\Delta W \approx$0.5 meV/Cu. This is a factor of 2 smaller than observed for Bi-2212[28] and a factor of 4 smaller than the one for Bi-2223.[31]

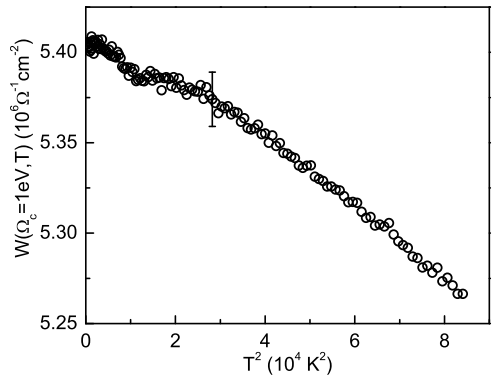

FIG. 10: (Color online) Integrated spectral weight for a cut off $\Omega_c = 1$ eV. The error bar indicates the estimated error due to the extrapolations used.

In order to separate the superconductivity induced changes from the temperature dependence of the normal state it is necessary to measure the changes in the optical constants as a function of temperature. Because the superconducting transition is second order, the superconductivity induced changes appear as a kink at T_c as can be seen in figure 11. A determination of the superconductivity induced spectral weight transfer by analysis of slope changes at T_c is more reliable since this method is much less sensitive to systematic errors in the absolute value of reflectivity. The details of this analysis are explained in Ref.[30]. The slope change at T_c for any optical quantity *f(ω,T)* is defined as,[30]

$$\Delta_s f(\omega) = \left(\frac{\partial f(\omega,T)}{\partial T}\right)_{T_c+\delta} - \left(\frac{\partial f(\omega,T)}{\partial T}\right)_{T_c-\delta}. \quad (8)$$

Since the slope changes are smeared due to fluctuations, the derivatives correspond to average values in certain regions δ above and below T_c. For this analysis one needs temperature dependencies with a dense sampling in temperatures. Figure 11 shows the measured temperature

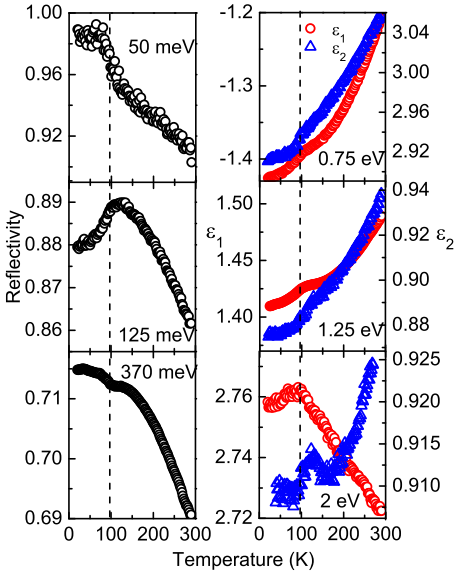

FIG. 11: Temperature dependencies of the in-plane reflectivity and dielectric function for selected energies. The dashed lines indicate T_c.

dependencies for selected photon energies. From these temperature dependencies the slope change at T_c can be estimated. Since numerical derivatives of the data are very noisy, the temperature dependencies are fitted above and below T_c to a second order polynomial.[30] The derivatives are then simply calculated from the analytical expressions. Figure 12 shows the slope change of the reflectivity and the dielectric function at T_c. The functions $\Delta_s R(\omega)$, $\Delta_s \epsilon_1(\omega)$ and $\Delta_s \epsilon_2(\omega)$ were obtained by fitting the data (figure 11) between 40 K and T_c (= 97 K) and between T_c and 200 K. The error bars were estimated by varying the upper and lower limits for both the high and low temperature fits.

From the inset of figure 12a one can see the good agreement between the slope change estimated from reflectivity and ellipsometric measurements. Spectra of $\Delta_s \epsilon_1$ and $\Delta_s \epsilon_2$ satisfy KK relations, therefore $\Delta_s \epsilon$ can be modelled with an oscillator model that has the same functional form as a Drude-Lorentz model,

$$\Delta_s \epsilon = \Delta_s \epsilon_\infty + \sum_{i=0}^{N} \frac{A_i}{\omega_i^2 - \omega^2 - i\gamma_i \omega} \qquad (9)$$

where $\Delta_s \epsilon_\infty$ is the change in the high energy contribution, ω_i is the center frequency of the ith oscillator, γ_i is its width and A_i is the oscillator strength. The difference with a normal Drude-Lorentz model is that the oscillator strength can take on both positive and negative values corresponding to the addition or removal of spectral weight. $\Delta_s \sigma(\omega)$ is easily calculated from $\Delta_s \epsilon$ and the slope difference integrated spectral weight is then defined as,

$$\Delta_s W(\Omega_c) = \frac{A_0}{8} + \int_{0+}^{\Omega_c} \Delta_s \sigma_1(\omega) d\omega \qquad (10)$$

with A_0 the condensate strength. This quantity is displayed in figure 12c. The result gives $\Delta_s W(\Omega_c) = +540$ $\Omega^{-1}\mathrm{cm}^{-2}K^{-1}$ for a cut off $\Omega_c \approx 1$ eV. This result is somewhat lower than that for Bi-2212 ($\Delta_s W(\Omega_c) = +770$ $\Omega^{-1}\mathrm{cm}^{-2}K^{-1}$)[30] and Bi-2223 ($\Delta_s W(\Omega_c) = +1100$ $\Omega^{-1}\mathrm{cm}^{-2}K^{-1}$)[31] but has the same sign and order of magnitude. It is also possible to calculate $\Delta_s W(\Omega_c)$ directly from the measured temperature dependence of $W(\Omega_c, T)$, by fitting $W(\Omega_c, T)$ in exactly the same way as is done for the other optical quantities. The result obtained in this way is $\Delta_{s,direct} W(\Omega_c) = +420 \pm 150$ $\Omega^{-1}\mathrm{cm}^{-2}K^{-1}$ which is a little bit lower but consistent with the result obtained using the temperature modulation analysis.

D. Specific heat anomaly

Figure 5b shows specific-heat data taken in different magnetic fields after subtracting the 14 Tesla data as a background. The specific heat in zero field clearly shows an asymmetric lambda shape typical for a superconducting transition governed by thermal fluctuations of the anisotropic 3D-XY universality class.[35,36] The shape of the anomaly shows more resemblance to that of optimally doped YBCO[37] than to that of the more two dimensional Bi-2212 which shows a symmetric anomaly.[38] As in YBCO,[37] the peak is clearly shifted to lower temperatures in a magnetic field. This shift is well described in the framework of 3D-XY fluctuations.[36] A contribution due to fluctuations can be seen up to ∼15 K above T_c. Since a 14 T field is by far not enough to suppress all pair correlations above T_c, there probably also is a contribution at higher temperatures which can not be observed with this method.[35,39] The influence of a magnetic field on the fluctuations is to introduce a magnetic length $l = (\Phi_0/B)^{1/2}$ closely related to the vortex-vortex distance which reduces the effective dimensionality.[36,39] In the critical 3D-XY regime, the correlation length diverges upon approaching T_c following a power law of the form $\xi \sim \xi_0(1-t)^{-\nu}$ with $t = T/T_c$ and ν=0.67 for the 3D-XY universality class. The presence of a magnetic length scale cuts off this divergence within a certain temperature window and thus broadens the transition in a field as seen in the specific heat data. The superconducting transition is thus far from being a BCS type transition where the transition temperature is reduced in a field because the Cooper pairs are broken up. Here T_c is rather a phase-ordering transition comparable to that of superfluid 4He, albeit with a clear anisotropy. Due to the lack of the exact phonon background it is not possible to estimate up to which temperatures fluctuations due to phase correlations of preformed Cooper pairs exist. However, it should be noted here that no anomaly at

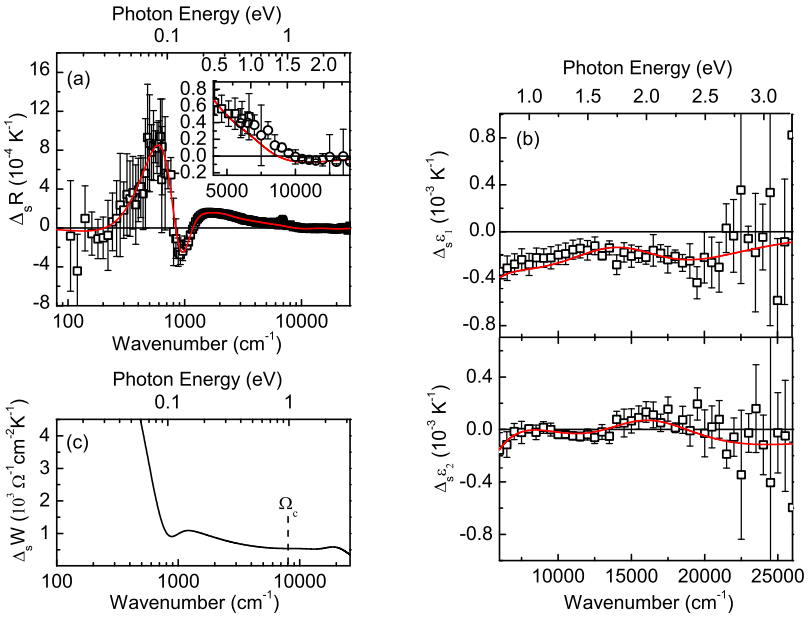

FIG. 12: Spectral dependence of (a): $\Delta_s R$ (squares), (b): $\Delta_s \epsilon_{1,2}$ (squares). Solid lines in (a) and (b) are the fits of the $\Delta_s R$ and $\Delta_s \epsilon_{1,2}$ spectra. The inset in (a) shows the excellent match between the directly measured $\Delta_s R$ (squares) and the $\Delta_s R$ calculated from $\Delta_s \epsilon_{1,2}$ (circles). (c): $\Delta_s W$ calculated from the best fit to $\Delta_s R$ and $\Delta_s \epsilon_{1,2}$ using Eq. 10. The observed spectral weight increase is $\Delta_s W(\Omega_c) = +540\ \Omega^{-1}\mathrm{cm}^{-2}K^{-1}$. The dashed line indicates the cut off frequency used to calculate W(Ω_c,T).

higher temperatures is visible, suggesting a rather continuous evolution of pair correlations at higher temperatures with a continuous opening of a superconducting gap far above T_c, whereas the lifetime of phase fluctuations is finite.[40] An interesting point is that a field of 14 T has a clear influence on the fluctuations above T_c (between 100 K and 115 K), while no effect of an applied field has been reported for YBCO.[37] This suggests a stronger pair breaking effect by a magnetic field and thus points to a smaller upper critical field in this compound. In a BCS type superconductor the specific heat in the normal and the superconducting state is used to evaluate the thermodynamic critical field $H_c(T)$ which is a measure of the condensation energy. In the presence of fluctuation contributions it has been argued that fluctuation contributions above T_c have to be considered to calculate the real condensation energy.[41] As the true phonon background is unknown here this calculation cannot be performed. Information can be obtained by comparing the size of the specific heat anomaly with that of other cuprate superconductors having a similar T_c. Nevertheless the specific heat jump $\Delta C = 0.052$ J gat^{-1} K^{-1} can be compared to $\Delta C = 0.2$ J gat^{-1} K^{-1} found for optimally doped Bi-2212[38] and $\Delta C = 0.46$ J gat^{-1} K^{-1} for overdoped YBCO[37] (the abbreviation gat stands for gramatom). The large difference to the value found in YBCO can be explained by the larger contribution of fluctuation above T_c in Hg-1201 (and Bi-2212) which appears to have a larger anisotropy and thus more 2D correlations above T_c. A large part of the condensation energy can thus be attributed to the smooth onset of 2D correlations of Cooper pairs far above T_c. The anomaly which is visible at T_c represents thus only a small part of the condensation energy.[41] If the units eV/K and data normalized per Cu-atom are used, the single layer compound can be compared to the 2-layer compound Bi-2212. This leads to ΔC=4.3·10^{-3} meV K^{-1} per copper for Hg-1201 which is 3.5 times smaller than the value found for optimally doped Bi-2212 ΔC=1.5·10^{-2} meV K^{-1} per copper.

From the specific heat we estimate the change in internal energy by integrating,

$$\Delta U(T) = \int_0^T [C(0T, T') - C(14T, T')]dT' \qquad (11)$$

Figure 13 shows a comparison between the internal energy relative to 60 K and the kinetic energy relative to 20 K defined as -$\delta W(T) = W(\Omega_c, T) - W(\Omega_c, T = 20K)$. We find that $\delta W(T)$ is about 3 times larger than the $\Delta U(T)$, so in principle $\delta W(T)$ is large enough to account for the condensation energy. We note again that the change in internal energy is probably only a small part of the condensation energy because the fields used here are by far not enough to completely suppress superconductivity. The temperature dependence of δW around T_c is much more gradual than the one for ΔU. Because of the better signal-to-noise ratio of the specific heat data it is possible to observe the change in internal energy due to the phase ordering transition as a rather sharp step at T_c. Superimposed on this is the much more gradual change due to the 2d fluctuations. Since the phase order-

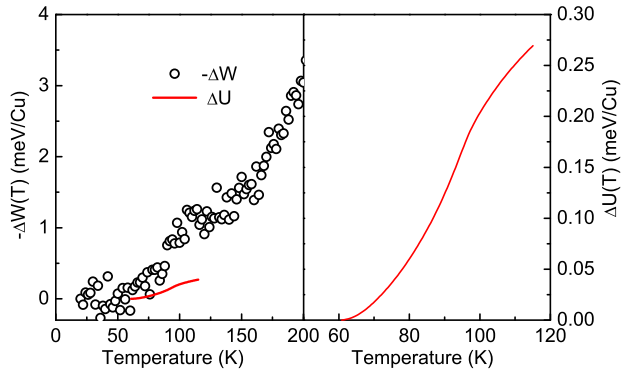

FIG. 13: Comparison between the kinetic energy relative to 20 K, -$\delta W(T) = W(\Omega_c, T) - W(\Omega_c, T = 20K)$ on the left and the internal energy $\Delta U(T)$ relative to 60 K on the right. The red line in the left panel is $\Delta U(T)$ plotted on the same scale as $\delta W(T)$.

ing transition occurs in a narrow window around T_c and contributes only a small part of the change in internal energy, we are probably not able to observe this change in $\delta W(T)$.

V. CONCLUSIONS

Optimally doped, single layer $HgBa_2CuO_{4+\delta}$ has been investigated using optical and calorimetric techniques. From an extended Drude analysis we find a reasonable agreement between the onset in absorption as seen in the optical measurements and the reported values for the gap and the resonance energy of the magnetic mode. We have presented detailed temperature dependencies of $m^*(\omega, T)/m_b$ and $1/\tau(\omega, T)$. The in-plane superfluid plasma frequency is found to be $\omega_{p,s} \approx 9600 \pm 400$ cm^{-1} whereas the out-of-plane $\omega_{p,s} \approx 290 \pm 10$ cm^{-1}. Both the in-plane and out-of-plane superfluid densities fall on the scaling relation of Ref[16]. From an analysis of the temperature dependent spectral weight W(Ω_c,T) we find that the low frequency spectral weight shows a superconductivity induced *increase*. The corresponding decrease in kinetic energy $\Delta W \approx$0.5 meV per copper is sufficient to explain the condensation energy extracted from the specific heat measurements. We observe a specific heat anomaly that is comparable in shape to YBCO and shows a similar field dependence, but has a size of the anomaly is 10 times smaller however.

VI. ACKNOWLEDGMENTS

We gratefully acknowledge stimulating discussions with F. Marsiglio. The work at the University of Geneva is supported by the Swiss National Science Foundation through the National Center of Competence in Research "Materials with Novel Electronic Properties-MaNEP". Work at Brookhaven was supported by the Office of Science, U.S. Department of Energy, under Contract No. DE-AC02-98CH10886. The crystal growth work at Stanford University was supported by the DOE under Contract No. DE-AC02-76SF00515 and by the NSF under Grant No. 0405655.

[1] X. Zhao *et al.*, To be published in Advanced Materials (cond-mat/0604103).
[2] L. Lu *et al.*, Phys. Rev. Let., **95**, 217003 (2005).
[3] W.S. Lee *et al.*, cond-mat/0606347.
[4] A.Pimenov, A. V. Pronin, A. Loidl, A. Tsukada, and M. Naito, Phys. Rev. B **66**, 212508, (2002).
[5] F. Wooten, Optical Properties of Solids (Academic Press, New York, 1972).
[6] N. Barisic, M. Greven, private communication.
[7] A. B. Kuzmenko, Rev. Sci. Instr., **76**, 083108 (2005).
[8] T. Timusk, Solid State Commun. **127**, 337 (2003).
[9] Y. Wang, A.T. Plackowski, A. Junod, Physica C **355**, 179 (2001).
[10] A. Carrington *et al.*, Czech. J. Phys. **46**, 3177 (1996).
[11] B. Billon, M. Charalambous, O. Riou, J. Chaussy, D. Pelloquin, Phys. Rev. B **56**, 10824 (1997).
[12] J.W. Allen and J. C. Mikkelsen, Phys. Rev. B **15**, 2952 (1977).
[13] A. El Azrak, R. Nahoum, N. Bontemps, M. Guilloux-Viry, C. Thivet, A. Perrin, S. Labdi, Z. Z. Li and H. Raffy, Phys. Rev. B **49**, 9846 (1994).
[14] D. van der Marel, H.J.A. Molegraaf, J. Zaanen, Z. Nussinov, F. Carbone, A. Damascelli, H. Eisaki, M. Greven, P.H. Kes, M. Li, Nature **425**, 271 (2003).
[15] J.Hwang, T. Timusk, G.D. Gu, Nature **427**, 714 (2004).
[16] C.C. Homes, S.V. Dordevic, T. Valla, and M. Strongin, Phys. Rev. B **72**, 134517 (2005).
[17] F. Marsiglio, F. Carbone, A.B. Kuzmenko, D. van der Marel, cond-mat/0606688.
[18] J. E. Hirsch, Physica C **199**, 305 (1992).
[19] P.W. Anderson, P.A. Lee, M. Randeria, T.M. Rice, N. Trivedi and F.C. Zhang, J. Phys.: Condens. Matter **16**, 755(R) (2004).
[20] T. Eckl, W. Hanke and E. Arrigoni, Phys. Rev. B **68**, 014505 (2003).
[21] P. Wróbel, R. Eder and P. Fulde, J. Phys.: Condens. Matter **15**, 6599 (2003).
[22] K. Haule and G. Kotliar, cond-mat/0601478.
[23] A. Toschi, M. Capone, M. Ortolani, P. Calvani, S. Lupi and C. Castellani, Phys. Rev. Lett. **95**, 097002 (2005).
[24] F. Marsiglio, Phys. Rev. B **73**, 064507 (2006)
[25] Th.A. Maier, M. Jarrell, A. Macridin, and C. Slezak, Phys. Rev. Lett. **92**, 27005 (2004).
[26] M.R. Norman, C. Pépin, Phys. Rev. B **66**, 100506(R) (2002)
[27] D.N. Basov, S.I. Woods, A.S. Katz, E.J. Singley, R.C.

Dynes, M.Xu, D.G. Hinks, C.C. Homes, M. Strongin, Science **283**, 49 (1999).
[28] H.J.A. Molegraaf, C. Presura, D. van der Marel, P.H. Kes, and M. Li, Science **295**, 2239 (2002).
[29] A.F. Santander-Syro, R.P.S. Lobo, N. Bontemps, Z. Konstatinovic, Z.Z. Li, H. Raffy. Europhys. Lett. **62**, 568 (2003).
[30] A.B. Kuzmenko, H.J.A. Molegraaf, F. Carbone, and D. van der Marel, Phys.Rev.B **72**, 144503 (2005).
[31] F. Carbone, A.B. Kuzmenko, H.J.A. Molegraaf, E. van Heumen, E. Giannini, D. van der Marel, Phys. Rev. B **74**, 24502 (2006).
[32] G. Deutscher, A.F. Santander-Syro and N. Bontemps, Phys. Rev. B **72** 092504 (2005).
[33] F. Carbone *et al.*, Phys. Rev. B **74**, 064510 (2006).
[34] A.B. Kuzmenko, D. van der Marel, F. Carbone, F. Marsiglio, in preparation.
[35] C. Meingast *et al.*, Phys. Rev. Lett. **86**, 1606 (2001).
[36] T. Schneider, J.M. Singer, *Phase Transition Approach to High Temperature Superconductivity*, Imperial College Press 2000.
[37] A. Junod, M. Roulin, J.Y. Genoud, B. Revaz, A. Erb, E. Walker, Physica C **275**, 245 (1997).
[38] A. Junod, K.Q. Wang, G. Triscone and J. Muller, Physica B **194-196**, 1497 (1994).
[39] R. Lortz, C. Meingast, A.I. Rykov, S. Tajima, Phys. Rev. Lett. **91**, 207001 (2003).
[40] J. Corson, R. Mallozzi, J. Orenstein, J.N. Eckstein and I. Bozovic, Nature **398**, 221 (1999).
[41] D. van der Marel, A.J. Leggett, J.W. Loram, J.R. Kirtley, Phys. Rev. B **66**, 140501(R) (2002).